Computer Aided Surgery 7:257–267 (2002)

Biomedical Paper

Automatic 3D Registration for Interventional MRI-Guided Treatment of Prostate Cancer

Baowei Fei, Ph.D., Jeffrey L. Duerk, Ph.D., and David L. Wilson, Ph.D.
Department of Biomedical Engineering, Case Western Reserve University (B.F., J.L.D., D.L.W.) and Department of Radiology, University Hospitals of Cleveland and Case Western Reserve University (J.L.D., D.L.W.), Cleveland, Ohio

ABSTRACT

The goal of this research is to register real-time interventional magnetic resonance imaging (iMRI) slice images with a previously obtained high-resolution MRI image volume, which in turn can be registered with functional images such as those from SPECT. The immediate application is in iMRI-guided treatment of prostate cancer, where additional images are desired to improve tumor targeting. In this article, simulation experiments are performed to demonstrate the feasibility of slice-to-volume registration for this application. We acquired 3D volume images from a 1.5-T MRI system and simulated low-field iMRI image slices by creating thick slices and adding noise. We created a slice-to-volume mutual information registration algorithm with special features to improve robustness. Features included a multiresolution approach, two similarity measures, and automatic restarting to avoid local minima. To assess the quality of registration, we calculated 3D displacements on a voxel-by-voxel basis over a volume of interest between slice-to-volume registration and volume-to-volume registration, which was previously shown to be quite accurate. More than 800 registration experiments were performed on MR images of three volunteers. The slice-to-volume registration algorithm was very robust and accurate for transverse slice images covering the prostate, with a registration error of only 0.4 ± 0.2 mm. Error was greater at other slice orientations and positions. The automatic slice-to-volume mutual information registration algorithm is robust and probably sufficiently accurate to aid in iMRI-guided treatment of prostate cancer. Comp Aid Surg 7: 257–267 (2002). ©2003 Wiley-Liss, Inc.

Key words: **image registration; mutual information; magnetic resonance imaging (MRI); interventional MRI; prostate cancer; minimally invasive treatment**

INTRODUCTION

We use a low-field open magnet system to guide minimally invasive treatments, including radiofrequency (RF) thermal ablation of abdominal cancer.[1–3] We are currently investigating the incorporation of other medical images for use in live-time treatment planning and execution. Examples of images for possible incorporation include high-resolution MR images from another scanner or from a

Received January 31, 2002; accepted October 16, 2002.

Address correspondence/reprint requests to: David L. Wilson, Ph.D., Department of Biomedical Engineering, Case Western Reserve University, 10900 Euclid Avenue, Cleveland, OH 44106. E-mail: dlw@po.cwru.edu; http://imaging.ebme.cwru.edu

Published online in Wiley InterScience (www.interscience.wiley.com). DOI: 10.1002/igs.10052

very-long-duration acquisition in the iMRI scanner, MR spectroscopy images, functional MR images, MR angiography images, PET images, and SPECT images. In some cases, these other images can be used to localize a disease process such as a tumor; in other cases, the images can be used to locate a structure that should be avoided, such as a critical brain structure identified with functional MRI. iMRI is currently under investigation for possible use in the treatment of prostate cancer. Because MRI does not reliably show prostate tumor, we intend to incorporate nuclear medicine or MR spectroscopy images with an improved ability to detect and localize the tumor.[4,5]

To incorporate image data from other sources in a real-time iMRI procedure, we intend to register two-dimensional (2D) slice images acquired quickly on the iMRI scanner with a previously acquired volume of image data. An image volume from another modality can then be registered with the full MR volume. Thus, to incorporate SPECT in an iMRI procedure, we will first register the SPECT image volume with an MR volume.[6] Then, when registering iMRI slice images to the MR volume, they can also be mapped to the SPECT functional image data. If this procedure is successful, a variety of potential visualization tools will be available to help the physician localize and apply treatments appropriately. The real-time iMRI images will be used for guidance, and any small misregistration errors can very probably be mentally corrected by the physician. To simplify and improve the slice-to-volume (SV) registration step, we intend to always use MR images acquired with similar pulse sequences. In this report, we investigate SV registration of MR images.

Previous success with registering one MR prostate volume to another[7] encourages us to pursue this plan. We call this process volume-to-volume or VV registration. A rigid-body mutual information registration method was used, with some features to improve robustness.[7] We carefully evaluated registration quality using a variety of methods. For volume pairs acquired over a short timespan from a supine subject with legs flat on the table, registration accuracy for both prostate centroids (typically <1 mm) and bony landmarks (average 1.6 mm) was in the order of one voxel (≈ 1.4 mm). For volumes acquired under very different conditions, for example, with legs flat or raised into the treatment position, or with and without bladder or rectal filling, we obtained somewhat larger prostate centroid registration errors of about 3.0 mm. From our results with VV prostate registration, it was decided that SV accuracy could be assessed by comparing results to VV registration for those volume pairs having low VV registration error.

SV registration is an alternative, fast approach for including other modalities in iMRI-guided treatment. Previously, image registration was used to combine preoperative MRI and CT volumes for iMRI-guided intranasal microendoscopy where iMRI volumes were acquired and registered with preoperative data.[8] Here, it is anticipated that the SV method will be faster, because image acquisition is faster and because registration of a slice should require many fewer calculations for a volume. In addition, our experience is that 2D slice acquisitions are routinely acquired during iMRI interventions, whereas volume acquisitions are only acquired infrequently. In previously published reports, SV registration was mainly applied to the brain for applications of functional MRI,[9,10] postmortem pathology studies,[11] and anatomical modeling.[12] There are no reports of SV registration for abdominal organs or iMRI guidance.

The application of SV registration methods to iMRI-guided treatment of prostate cancer raises several challenges. First, iMRI images often have a lower signal-to-noise ratio (SNR) than diagnostic MR images because of the emphasis on fast imaging and because of the typically lower field-strength of open iMRI magnets. Second, a single slice, or a few slices, provides many fewer structures than an entire volume for voxel-based matching. Third, the prostate can move relative to the pelvic bones due to changes in rectal and bladder filling[13,14] or changes in patient posture for treatment.[7] That is, alignment of the pelvic bones (prominent anatomical features in MR gray-scale images) does not necessarily ensure that the prostate is aligned. Fourth, the normal prostate is a small organ; when healthy, it measures only ~ 3.8 cm in its widest dimension.[15] The prostate is located below the much larger bladder, which can change its shape and size during imaging. Finally, times for registration and algorithm robustness are of particular concern in this application.

In this study, we test the performance of SV registration. In the next section, we first describe a voxel-based registration method with special features to improve robustness. This is followed by details of how entire MR volume pairs are acquired on a conventional MR scanner and how realistic iMRI images are simulated. Later, results are presented from over 800 registration experiments comparing slice-to-volume with volume-to-volume registration.

MATERIALS AND METHODS

Registration Algorithm

We used an algorithm with special features for the slice-to-volume, or SV, registration. A similar algorithm was previously successfully applied to MR volume-to-volume registration of the prostate.[7] The algorithm is outlined in the following paragraphs.[7,16]

We used two similarity measures, mutual information (MI) and correlation coefficient (CC), in the registration. One image, R, is the *reference*, and the other, F, is *floating*. Their mutual information $MI(R, F)$ is given below.[17]

$$MI(R, F) = \sum_{r,f} P_{RF}(r, f) \log \frac{p_{RF}(r, f)}{p_R(r) \cdot p_F(f)}$$

The joint probability, $p_{RF}(r, f)$, and the marginal probabilities of the reference image, $p_R(r)$, and the floating image, $p_F(f)$, can be estimated from the normalized joint intensity histogram. The correlation coefficient $CC(R, F)$ is given below.[18]

$$CC(R, F) = \frac{\sum (R(r) - \bar{R}(r))(F(f) - \bar{F}(f))}{\sqrt{\sum (R(r) - \bar{R}(r))^2 \sum (F(f) - \bar{F}(f))^2}}$$

Here, $\bar{R}(r)$, $\bar{F}(f)$ denote the average intensities of the reference and floating images, respectively, and the summation includes all voxels within the overlap region.

We compared the two similarity measures at different resolutions to determine their suitability for SV registration. At $\frac{1}{4}$ resolution, we resampled images so as to give one-quarter the number of voxels along each linear dimension. At *full resolution*, we used the full number of voxels. In Figure 1, the two similarity measures are plotted as a function of translations. Two high-resolution MR volumes were registered as described previously,[7] and values were plotted with the origin as the optimal transformation. We calculated CC and MI values while moving the simulated iMRI image relative to the high-resolution MR image along the coronal (anterior–posterior) axis. The simulated iMRI image was obtained as described later.

We use a multiresolution approach and perform registration from low to high resolution. We use CC at the two lower resolutions because it gives fewer local maxima (Fig. 1) and can be calculated faster than MI. We use MI at full resolution because the peaked similarity function gives a more precise solution than CC (Fig. 1). To avoid local maxima, we include a restarting feature where registration is restarted with randomly perturbed parameters obtained from a uniform distribution about the initial transformation values at the current resolution being used. The algorithm restarts until the absolute CC is above an experimentally determined threshold or the maximum number of restarts is reached. Absolute CC is used rather than MI because it has a well-defined range between 0 and 1, and because it provides an independent check of the MI result at the highest resolution.

All important results are recorded following an optimization cycle, including the CC and/or MI values, the number of restarts, and the transformation parameters. At the end of processing at a lower resolution, we always select the transformation parameters having the maximum CC value. We then scale the translation parameters appropriately and assign the new parameters to be initial values at the next-higher resolution. At the highest resolution, MI rather than CC is the similarity measure, and we select the final transformation parameters to be those with the maximum MI value.

For registration, we use rigid-body transformation (three translations and three rotations) and trilinear interpolation, as described previously.[19] For optimization, we use the downhill simplex method of Nelder and Mead.[20] Optimization of similarity ends either when the maximum number of calculations is reached (typically 500) or when the fractional change in the similarity function is smaller than a tolerance (typically 0.001). There are several preprocessing details to note: The input MRI volume is a 3D MR acquisition giving $256 \times 256 \times 128$ nearly isotropic voxels over a field of view covering the whole pelvis. We create isotropic voxels of about 1.37 mm on each side using 3D linear interpolation. IDL (Interactive Data Language, Research System Inc., Boulder, CO) is used as the programming language.

Typical parameter values are now described. An initial guess is used at the lowest resolution of all zeros because the patient is normally oriented approximately the same way from one scan to the next. All CC thresholds are set at 0.5, and the maximum number of restarts is set at 20, 10, and 5, from low to high resolution, respectively.

Image Acquisition

High-resolution MRI volumes were acquired using a 1.5-T Siemens MRI system (Magnetom Symphony, Siemens Medical Systems, Erlangen, Germany). An eight-element phased-array body coil was

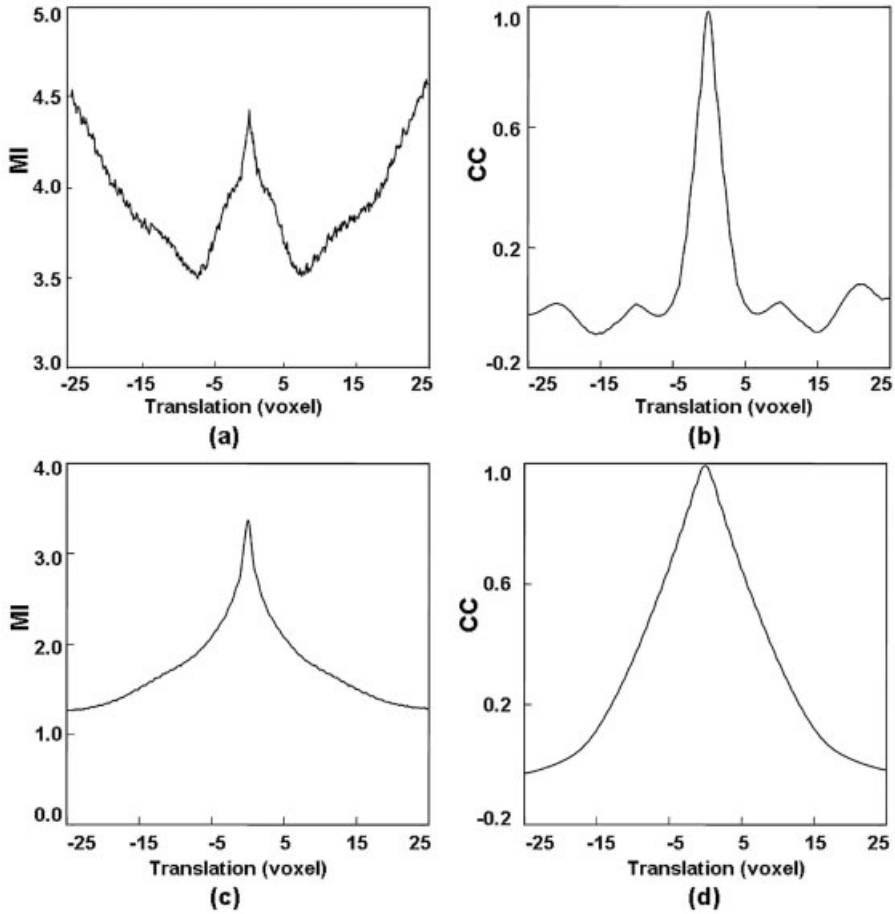

Fig. 1. Similarity functions are plotted as a function of translations in the multiresolution registration process. Two high-resolution MRI volumes were registered. From the optimal parameters, we computed the similarity of the simulated iMRI and MRI images as a function of translations along the coronal (anterior–posterior) axis. MI is plotted in (a) and (c); CC is plotted in (b) and (d). Graphs (a) and (b) are at the lowest resolution where images are down-sampled by 1/4 along each linear dimension, giving a distance between voxel centers of ~5.5 mm. A false global maximum for MI occurred at +25 voxels. Graphs (c) and (d) are plots at full resolution. Images are from volunteer S2.

used to ensure coverage of the prostate with a uniform sensitivity. Typically, two anterior and two posterior elements were enabled for signal acquisition.

Two different MR sequences were used. The first was a 3D RF spoiled gradient echo steady-state pulse sequence (FLASH) with TR/TE/flip parameters of 12/5.0/60, giving 256 × 256 × 128 voxels over a 330 × 330 × 256-mm field of view (FOV) to yield 1.3 × 1.3 × 2.0-mm voxels oriented to give the highest resolution for transverse slices. The acquisition time is 5.6 min. This sequence is good for pelvic imaging, but is not ideal for the prostate. It was used to acquire volumes for volunteer S1.

The second sequence was a 3D rapid gradient echo sequence (PSIF) designed to acquire the spin-echo component of the steady-state response, rather than the free induction decay. The spin-echo component forms immediately prior to the RF pulse, and is shifted toward the prior RF pulse through appropriate gradient waveform design. The sequence with 9.4/5.0/60 (TR/TE/flip) yields 160 × 256 × 128 voxels over a 219 × 350 × 192-mm rectangular FOV and 1.4 × 1.4 × 1.5-mm voxels oriented to give the highest resolution for transverse slices. There is oversampling at 31% in the slice direction to reduce aliasing artifacts. The acquisition time is 4.3 min. This sequence gave excellent image contrast for the prostate, and was used to acquire volumes for volunteers S2 and S3.

Imaging Experiments

We acquired high-resolution MRI volumes from three volunteers. For each volunteer, three image volumes were obtained with an imaging session.

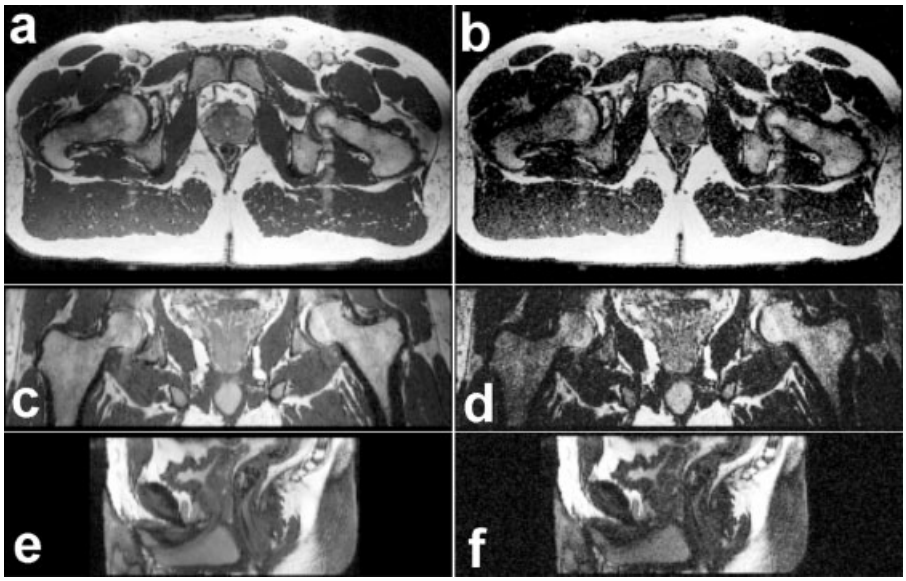

Fig. 2. Simulated iMRI images. Images on the left, (a), (c), and (e), are the original high-resolution MR images in the transverse, coronal, and sagittal planes, respectively. Images on the right are corresponding simulated thick iMRI images with SNR = 10. Images are from volunteer S2.

Each volume was acquired with compatible conditions. Volunteers laid supine with legs flat, similar to the position in routine MR scanning. Between volume acquisitions, volunteers got off the MRI table, stretched, and walked around to ensure that they would assume a different position when they laid back on the table. The coil array was centered on the prostate. All images of a volunteer were acquired with the same MRI acquisition parameters. In total, there were nine pairs of high-resolution MRI volumes for registration.

Simulation of iMRI Slice Images

We used high-resolution MRI volumes to simulate iMRI images by creating thick slices and adding noise and receive-coil inhomogeneity. Clinically, we typically use an iMRI slice thickness of 4.0–6.0 mm. We averaged three slices 1.4 mm thick to create a 4.2-mm-thick slice.

Noise was added to the simulated iMRI image. MR noise is described by the Rician distribution,[21] but at reasonably high signal values it is accurately approximated with Gaussian white noise.[22] We measured typical signal and noise values on our open magnet system using a homogenous phantom and methods described elsewhere.[23,24] Gaussian noise was then added to the simulated iMRI slice images either to match the measured SNR or to give much greater noise to further stress registration. We report noise experiments using the SNR of the simulated slice images. Figure 2 shows high-resolution MRI and noisy simulated iMRI slice images.

We simulated receive-coil inhomogeneity from a belt coil used in the clinical iMRI acquisitions. The coil is modeled as a solenoid, and the magnetic field is highest at the coil center, falling off in the axial direction. According to the Biot-Savart law,[25] this model also accounts for the spatial sensitivity of the coil to MR signal sources.

Registration Experiments

We desire an iMRI slice imaging method that gives robust, accurate registrations, and is relatively insensitive to acquisition parameters. Experiments were perfomed to determine the dependence on slice orientation (transverse, sagittal, and coronal), on slice position relative to the prostate (above, centered, and below), and on image noise from fast imaging techniques. For each volume pair, we extracted data from one volume and registered slice images to the other volume. Many different slices were used in experiments. Slice images are simulated as described above.

Registration Evaluation

Visual Inspection

Registration experiments were evaluated by visual inspection. We used *RegViz,* a program created in

IDL in our laboratory with multiple visualization and analysis methods. First, we manually segmented prostate boundaries in image slices and copied them to corresponding slices. This enabled visual determination of the overlap of prostate boundaries over the entire volume. Second, color overlay displays were used to evaluate overlap of structures. One image was rendered in gray and the other in the "hot iron" color scheme available in IDL. To visualize potential differences, it was useful to interactively change the contribution of each image using the transparency scale. Third, we used a sector display that divided the reference and registered images into rectangular sectors and created an output image by alternating sectors from the two input images. This way, even subtle shifts of edges would be clearly seen.

Comparison to Volume-to-Volume Registration Standard

Our standard evaluation method was to compare SV and VV registration. Because this relies on VV registration accuracy, we will now review our previous results.[7] For volume pairs acquired over a short time-span from a supine subject with legs flat on the table, prostates were well aligned, and prostate centroid displacements were typically <1 mm. The registration accuracy, as determined from displacements of pelvic bony landmarks, was 1.6 ± 0.2 mm. This error might be overestimated because it includes the uncertainty of locating the bony landmarks. The centroid error was slightly smaller because the prostate was at the volume center and rotation errors had less effect. From our success with VV prostate registration, it was decided that we could obtain SV accuracy by comparison with VV registrations for those volume pairs having low VV registration error.

To compare SV and VV registration, we defined a rectangular volume of interest (VOI) that just covered the prostate and calculated voxel displacements between the two registrations. To voxels within this VOI, we applied the transformations obtained by VV and SV registrations. We then calculated the 3D displacements between the transformed voxels. The mean voxel distance was used as the metric of SV registration error. For the evaluation of algorithm robustness, we defined the SV registration as being *successful* when the 3D displacement was less than 2.0 mm.

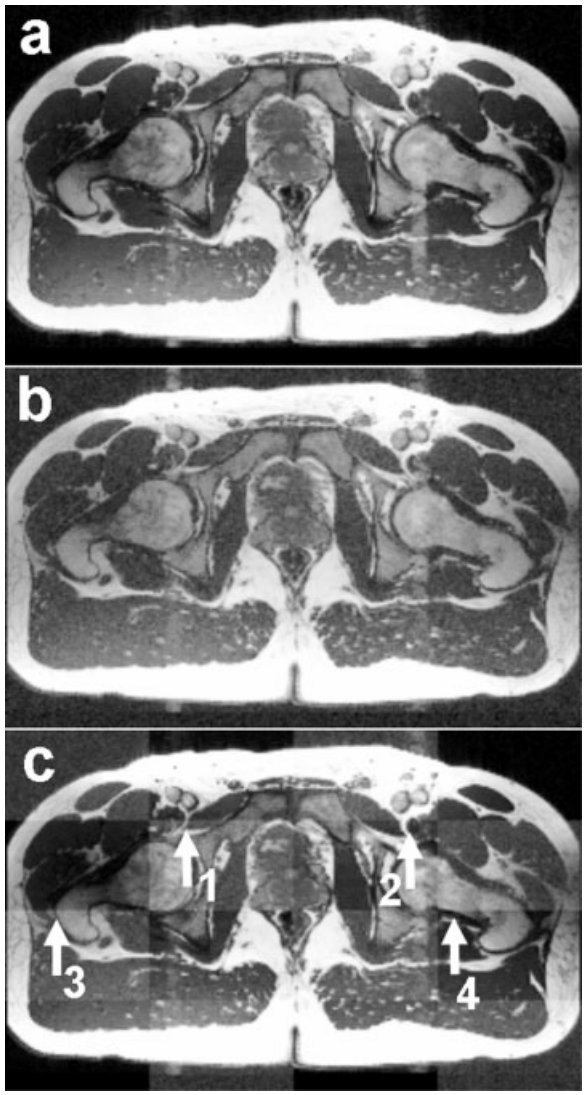

Fig. 3. Sector display showing excellent pelvic registration. Image (a) is a transverse slice from a high-resolution MRI volume. Image (b) is the corresponding noise iMRI slice. In the sector display shown in (c), alternating rectangular sections from (b) are made brighter and combined with sections from (a) to show the matching boundaries. The boundaries of bones and other structures are continuous, as shown particularly at locations 1–4. Other slices from this volume were also perfectly aligned, indicating good 3D alignment. Image volumes are from Volunteer S2.

RESULTS

Slice Orientation

In Figure 3, the sector display shows a simulated slice image registered with a high-resolution volume image. The slice image was obtained at a transverse orientation near the center of the prostate. The sector display shows excellent alignment

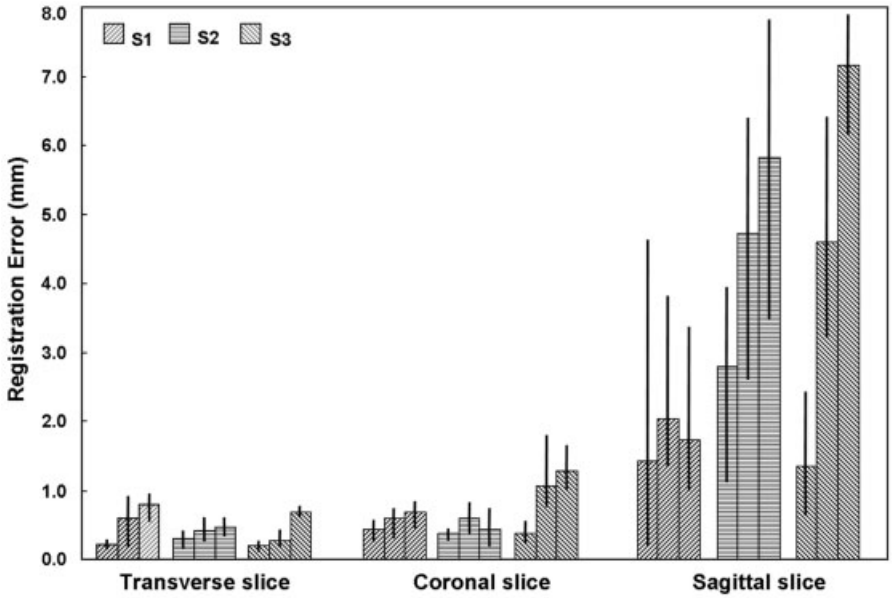

Fig. 4. SV registration using slices at different orientations. The error metric is the voxel displacement between the SV and VV transformations. Plotted are mean errors, as well as maxima and minima over a rectangular VOI surrounding the prostate. For each volunteer, S1, S2, and S3, we registered three volume pairs. For each pair, five registration experiments were conducted using five different simulated iMRI transverse slices intersecting the prostate. The simulated SNR was 25. Averaging data across all volunteers gives 0.4 ± 0.2 mm, 0.5 ± 0.2 mm, and 2.6 ± 1.6 mm errors for transverse, coronal, and sagittal slices, respectively.

at this position. Other transverse images were also well aligned, indicating that the registration was successful in three dimensions.

Figure 4 shows results for single slices oriented in the three traditional orthogonal directions. All slices are near the center of the prostate. Compared to VV transformations, registration error is smallest for transverse slices and largest for sagittal slices. Averaging across all transverse data, the error is only 0.4 ± 0.2 mm, where the latter number is a standard deviation. Coronal slices also gave quite small errors of 0.5 ± 0.2 mm. As shown in Figure 5c, transverse slices work best because they contain abundant anatomical structures that do not deform relative to the prostate. That is, a transverse slice centered at the prostate excludes the bladder that can deform and create an inconsistent match for registration. Figure 5a,b shows that coronal and sagittal views contain large regions of the bladder and rectum that can deform with filling. The following analyses are all based on transverse slices.

Slice Position

Figure 6 shows registration results for transverse slices at different distances from the prostate center. Slices centered on the prostate produced the best results, with a displacement error always less than 1.0 mm. The reason is that slices centered at the prostate include an abundance of bony structures giving good information for registration. They also exclude portions of the bladder that can deform and create inconsistent matches for registration (Fig. 7). Slices above the prostate include the deformable bladder, which can stress the registration algorithm, especially for volunteer S3 (Fig. 6). Slices below the prostate mainly contain muscle and fatty regions from the hips that can deform, and there is less information for rigid-body registration. This effect was more pronounced for volunteer S2 (Fig. 6).

Noise Level

Figure 8 shows registration results for transverse slices with added noise. The typical iMRI SNR under clinical conditions is about 25. Even when noise far exceeded this normal situation, registration results were still quite good. A 100% success rate was achieved with an acceptance criterion of <2.0 mm, even when the SNR was as bad as 10.

Robustness and Calculation Time

The registration algorithm was quite robust for transverse slices covering the prostate. Using the

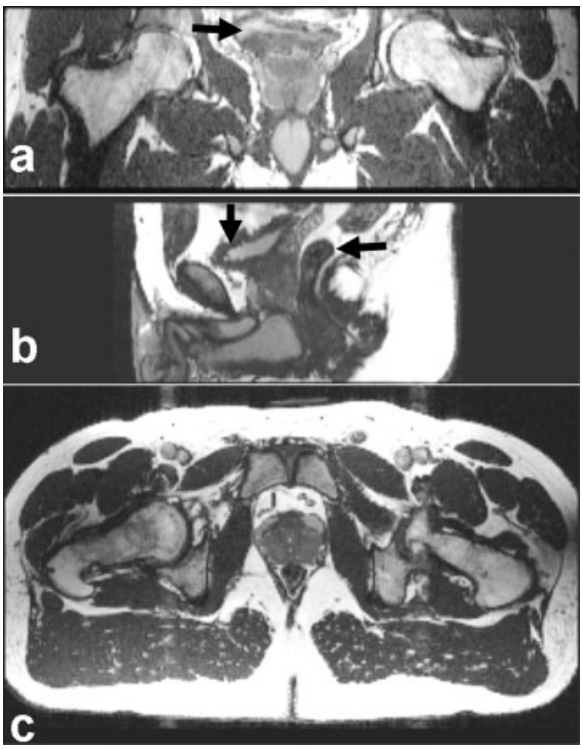

Fig. 5. Image slices showing the advantage of transverse images. The coronal slice in (a) contains the bladder, as indicated by the black arrow. The sagittal slice in (b) contains both the bladder (vertical arrow) and rectum (horizontal arrow). The transverse slice in (c) excludes the bladder and contains abundant bony structures.

nine volume pairs from three volunteers, the algorithm never failed for any transverse slice covering the prostate. In addition, the final registration result was insensitive to initial guesses within a large range: [−60, +60] mm for translations and [−20, +20] degrees for rotations. With the restarting algorithm, we even successfully registered slices as much as 80 mm from the optimum. This working range is probably sufficient for clinical applications where we can ensure good starting values. Using the pelvic bones as markers and needle localization methods,[26] we should be able to position the prostate within about ±20 mm. In addition, the patient normally lies supine in the MR bed with very little rotation (<±5 degrees).

The time for an SV registration was typically about 5 s on a Pentium IV 1.8-GHz CPU with 1 GB of memory. The algorithm was written in IDL and could probably be made much faster in a lower-level language such as C. A call to the simplex optimization typically resulted in 50 to 105 similarity evaluations before the tolerance value (0.001) was reached.

DISCUSSION

For transverse slices covering the prostate, the slice-to-volume registration results agreed very favorably with the volume-to-volume results. That is,

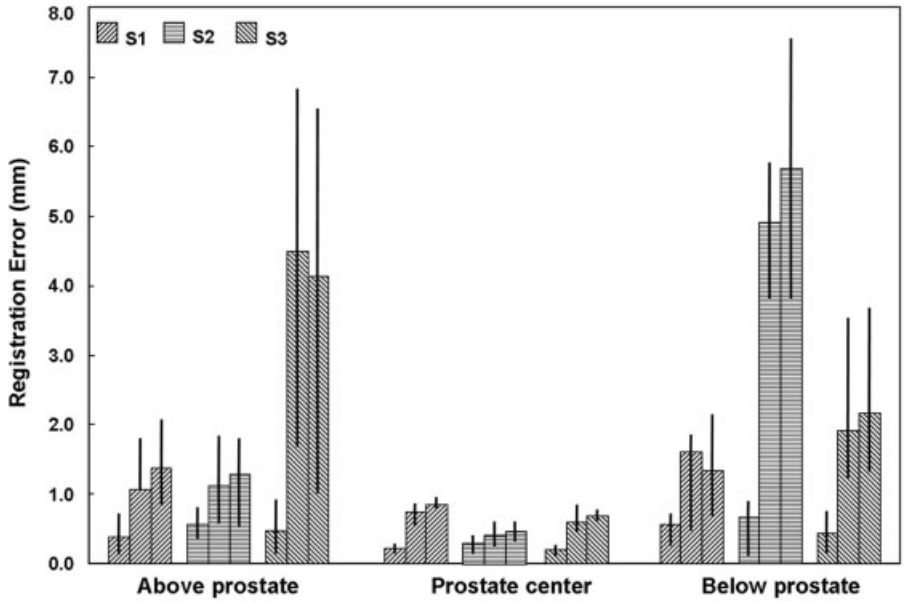

Fig. 6. SV registration using transverse slices at different positions. Groups of five iMRI slices each were extracted near the prostate center, ~35 mm above the prostate base, and ~35 mm below the prostate apex and registered to the MR volume. Other details are given in Figure 4. Slices at the prostate center worked best.

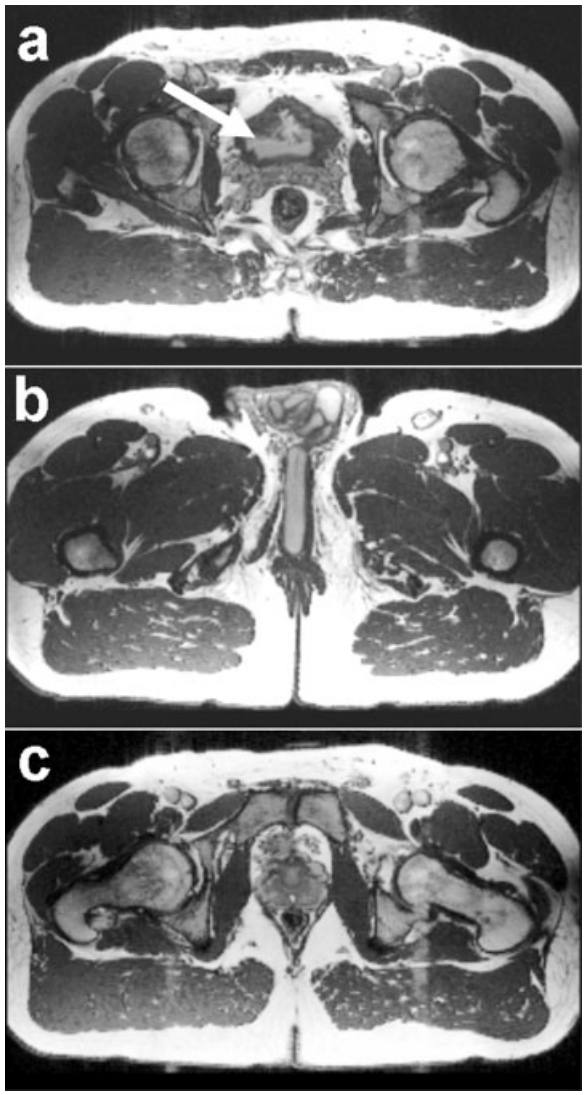

Fig. 7. Transverse images at different positions relative to the prostate. The image 35 mm above the prostate in (a) includes the bladder, indicated by the white arrow. A slice 35 mm below the prostate in (b) mainly contains muscle (dark) and fatty regions (white). A slice centered at the prostate in (c) has abundant bony structures.

we found that SV is equal to VV registration, with an average voxel displacement between them of only 0.4 mm in the prostate. The accuracy of SV is essentially the same as that previously reported for VV registration.[7] In our previous report, it was found that, whenever the subject was in comparable conditions, the prostate centroid registration error was typically <1 mm, or less than a voxel of 1.4 mm. Hence, for SV applied to images in this report, we predict a prostate error of very nearly 1.4 mm or less. In the previous report, it was found that whenever supine subjects raised their legs, the prostate moved towards the posterior direction by about 3 mm.[7] Another factor that affects prostate registration is rectal filling.[7,13] Hence, we recommend that prostate registration be done with the patient under similar conditions by maintaining a similar posture and by taking clinical measures to reduce rectal and bladder filling. We see no reason to suspect that SV registration would not be very accurate in these cases.

Slice-to-volume registration is probably sufficiently accurate for many iMRI applications. Compared to a typical iMRI slice thickness of $\sim$3.0 mm, SV registration is quite accurate. The accuracy of SV is probably much better than that of multimodality registration, where the typical functional image has a thickness of 3.0–4.0 mm. If one were to use functional or high-resolution MR images directly for targeting, the requirements for registration accuracy would be great. However, fused image data will not be used blindly. Rather, one can use fused images as a guide. Physicians will always use the real-time anatomical iMRI images for needle guidance.[26,27] With proper visualization tools, they should be able to mentally account for any small registration errors. In addition, there is very often image evidence of cancer in MR prostate images that can perhaps be identified with the aid of functional images. Such MR-visible lesions can become the markers for tumor targeting. As a result of these considerations, we believe that the accuracy of SV registration is sufficient to justify further investigation of its application in iMRI.

The algorithm is quite robust for the SV registration. Significantly, the registration never failed for transverse slices covering the prostate. It was obtained even in the presence of noise levels far beyond those encountered in iMRI. This is very important for iMRI, where magnetic fields are low and imaging is fast. It was also determined that coronal images work fairly well. This could be useful, because two orientations might provide more flexibility for clinical applications.

There are several reasons for the robustness. First, using both CC and MI at different resolutions was an important feature that increased robustness. When only MI was used, registrations at low resolution very often gave false solutions that misled registration at the next-highest resolution. Fortunately, CC performed well and gave many fewer local maxima at low resolution.[7] However, MI gave a more accurate solution at high resolution due to the peaked MI surface.[7] Our registration algorithm combined advantages from the two similarity mea-

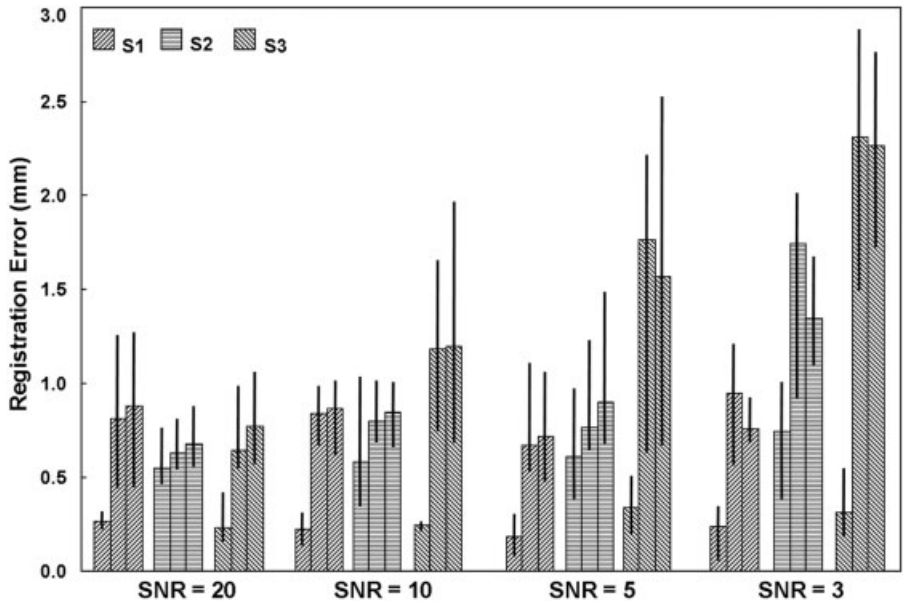

Fig. 8. SV registration at different noise levels. The simulated iMRI image slice had SNR values of 20, 10, 5, and 3, corresponding to added noise levels of 4, 8, 16, and 27 standard deviation gray levels, respectively. The transverse slices from Figure 4 were used. Other details are given in the legend of Figure 4. Even though noise greatly exceeds that found in iMRI, registration was little affected.

sures. Second, the restarting mechanism was also quite important. Without restarting, it was found that registrations sometimes failed in cases of volumes with a large mismatch of 54 mm and high noise. Even these cases resulted in a proper solution when restarting was employed.

The simulation provided a realistic, simple, and efficient way to evaluate the algorithm for our application. The simulated iMRI images are good representations of images from our low-field-strength iMRI system. However, there are other practical aspects of iMRI imaging that were not covered in the simulations. For instance, we did not reproduce the susceptibility artifact of an RF treatment needle in our simulations. From previous experience,[19] we think this is not a problem, because the needle artifact occupies a relatively small percentage of voxels in most cases.

Another practical aspect is possible deformation in the pelvic region. When images were acquired under much different conditions, such as supine or with legs raised, it was determined that warping was required to successfully register the prostate.[28,29] The warping registration method was based upon independent optimization of many interactively placed control points using MI and a thin-plate spline transformation. About 180 strategically placed control points were sufficiently expressive to capture important features of the deformation. In the event that a device such as an endorectal MR coil is used, warping registration will be required.

Finally, we conclude that the slice-to-volume registration algorithm is quite robust for transverse slice images covering the prostate, and that registration accuracy is probably sufficiently accurate to aid iMRI-guided thermal ablation of prostate cancer. It is quite feasible to include previously acquired high-resolution MRI or nuclear images in iMRI-guided treatment procedures, and we are beginning to explore this application in animal experiments.

ACKNOWLEDGMENT

Part of this work was presented at the SPIE Medical Imaging 2001 meeting in San Diego, California, February 2001. The algorithm developed in this research was supported by NIH Grants R01-CA84433-01 to D.L.W., and DOD Grant DAMD17-02-1-0230 to B.F. Imaging techniques were developed under the support of NIH Grant R33-CA88144-01 to J.L.D.

REFERENCES

1. Lewin JS, Connell CF, Duerk JL, Chung YC, Clampitt ME, Spisak J, Gazelle GS, Haaga JR. Interactive MRI-

guided radiofrequency interstitial thermal ablation of abdominal tumors: clinical trial for evaluation of safety and feasibility. J Magn Reson Imaging 1998;8:40–47.
2. Merkle EM, Shonk JR, Zheng L, Duerk JL, Lewin JS. MR imaging-guided radiofrequency thermal ablation in the porcine brain at 0.2T. Radiology 1999;213P: 1131.
3. Wilson DL, Carrillo A, Zheng L, Genc A, Duerk JL, Lewin JS. Evaluation of 3D image registration as applied to MR-guided thermal treatment of liver cancer. J Magn Reson Imaging 1998;8:77–84.
4. Sodee DB, Malguria N, Faulhaber P, Resnick MI, Albert J, Bakale G. Multicenter ProstaScint imaging findings in 2154 patients with prostate cancer. Urology 2000;56:988–993.
5. Scheidler J, Hricak H, Vigneron DB, Yu KK, Sokolov DL, Huang LR, Zaloudek CJ, Nelson SJ, Carroll PR, Kurhanewicz J. Prostate cancer: localization with three-dimensional proton MR spectroscopic imaging—clinicopathologic study. Radiology 1999;213:473–480.
6. Lee Z, Sodee DB, Duerk JL, Nelson AD, Berridge MS. Automatic registration of SPECT-MRI in the pelvis. J Nuclear Med 2000;41:232.
7. Fei BW, Wheaton A, Lee Z, Duerk JL, Wilson DL. Automatic MR volume registration and its evaluation for the pelvis and prostate. Phys Med Biol 2002;47: 823–838.
8. Hill DLG, Langsaeter LA, Poynter-Smith PN, Summers PE, Keevil SF, Walsh R, Hawkes DJ, Gleeson MJ. Feasibility study of magnetic resonance imaging-guided intranasal flexible microendoscopy. Comp Aid Surg 1997;2:264–275.
9. Kim B, Boes JL, Bland PH, Chenevert TL, Meyer CR. Motion correction in fMRI via registration of individual slices into an anatomical volume. Magn Reson Med 1999;41:964–972.
10. Rohlfing T, West JB, Beier J, Liebig T, Taschner CA, Thomale UW. Registration of functional and anatomical MRI: accuracy assessment and application in navigated neurosurgery. Comp Aid Surg 2000;5:414–425.
11. Kim TS, Singh M, Sungkarat W, Zarow C, Chui H. Automatic registration of postmortem brain slices to MRI reference volume. IEEE Trans Nuclear Sci 2000; 47:1607–1613.
12. Zhengping J, Mowforth PH. Mapping between MR brain images and voxel model. Med Inform (Lond) 1991;16:183–193.
13. Herk MV, Bruce A, Kroes APG, Shouman T, Touw A, Lebesque JV. Quantification of organ motion during conformal radiotherapy of the prostate by three dimensional image registration. Int J Radiat Oncol Biol Phys 1995;33:1311–1320.
14. Tenhaken RK, Forman JD, Heimburger DK, Gerhardsson A, McShan DL, Pereztamayo C, Schoeppel SL, Lichter AS. Treatment planning issues related to prostate movement in response to differential filling of the rectum and bladder. Int J Radiat Oncol Biol Phys 1991;20:1317–1324.
15. Gray H. Anatomy, Descriptive and Surgical. New York: Gramercy Books, 1977. p 1010.
16. Fei BW, Wheaton A, Lee Z, Nagano K, Duerk JL, Wilson DL. Robust registration algorithm for interventional MRI guidance for thermal ablation of prostate cancer. In: Mun SK, editor: Proceedings of SPIE Medical Imaging: Visualization, Display, and Image-Guided Procedures 2001. SPIE Vol 4319. p 53–60.
17. Collignon A, Maes F, Delaere D, Vandermeulen D, Suetens P, Marchal G. Automated multimodality image registration using information theory. In: BizaisY, Barillot C, DiPaola R, editors: Information Processing in Medical Imaging: Proceedings of 14th International Conference (IPMI'95). Computat Imaging Vis 1995. p 287–298.
18. Press WH, Teukolsky SA, Vellerling WT, Flannery BP. Numerical Recipes in C: The Art of Scientific Computing (2nd ed.). New York: The Press Syndicate of the University of Cambridge, 1992. p 636.
19. Carrillo A, Duerk JL, Lewin JS, Wilson DL. Semiautomatic 3-D image registration as applied to interventional MRI liver cancer treatment. IEEE Trans Med Imaging 2000;19:175–185.
20. Nelder J, Mead RA. A simplex method for function minimization. Comput J 1965;7:308–313.
21. Macovski A. Noise in MRI. Magn Reson Med 1996; 36:494–497.
22. Gregg RC, Nowak RD. Noise removal methods for high resolution MRI. IEEE Nuclear Sci Symp 1997; 2:1117–1121.
23. Henkelman RM. Measurement of signal intensities in the presence of noise in MR images. Med Phys 1985; 12:232–233.
24. Kaufman L, Kramer DM, Crooks LE, Ortendahl DA. Measuring signal-to-noise ratios in MR imaging. Radiology 1989;173:265–267.
25. Forbes LK, Crozier S, Doddrell DM. Rapid computation of static fields produced by thick circular solenoids. IEEE Trans Magnet 1997;33:4405–4410.
26. Lewin JS, Duerk JL, Jain VR, Petersilge CA, Chao CP, Haaga JR. Needle localization in MR-guided biopsy and aspiration: effects of field strength, sequence design, and magnetic field orientation. Am J Roentgenol 1996;166:1337–1345.
27. Merkle EM, Shonk JR, Zheng L, Duerk JL, Lewin JS. MR imaging-guided radiofrequency thermal ablation in the porcine brain at 0.2 T. Eur Radiol 2001;11:884–892.
28. Fei BW, Kemper C, Wilson DL. Three-dimensional warping registration of the pelvis and prostate. In: Sonka M, Fitzpatrick JM, editors: Proceedings of SPIE Medical Imaging Image Processing 2002. SPIE Vol 4684. p 528–537.
29. Fei BW, Kemper C, Wilson DL. A comparative study of warping and rigid body registration for the prostate and pelvic MR volumes. Comp Med Imaging and Graphics 2003 (in press).

Fei BW, Duerk JL, Wilson DL. Automatic 3D registration for interventional MRI-guided treatment of prostate cancer. Computer Aided Surgery 2002;7:257-267.